CHEMISTRY OF MATERIALS

ARTICLE

pubs.acs.org/cm

Donor−Acceptor−Donor-based π-Conjugated Oligomers for Nonlinear Optics and Near-IR Emission

Stefan Ellinger,[†] Kenneth R. Graham,[†] Pengjie Shi,[†] Richard T. Farley,[†] Timothy T. Steckler,[†] Robert N. Brookins,[†] Prasad Taranekar,[†] Jianguo Mei,[†] Lazaro A. Padilha,[‡] Trenton R. Ensley,[‡] Honghua Hu,[‡] Scott Webster,[‡] David J. Hagan,[‡,§] Eric W. Van Stryland,[‡,§] Kirk S. Schanze,[†] and John R. Reynolds*[,†]

[†]Department of Chemistry, Center for Macromolecular Science and Engineering, University of Florida, Gainesville, Florida 32611, United States

[‡]CREOL, The College of Optics and Photonics, [§]Department of Physics, University of Central Florida, 4000 Central Florida Boulevard, Orlando, Florida 32816, United States

Supporting Information

ABSTRACT: A family of multi-heterocycle donor−acceptor−donor (DAD) telechelic conjugated oligomers designed for two-photon absorption (2PA) and emission in the near-infrared (near-IR) were prepared, and the relationship between their spectral, structural, and electrochemical properties were investigated. These oligomers, based on electron-rich thiophene, phenylene, and 3,4-ethylenedioxythiophene (EDOT) units as donors along with electron-deficient benzothiadiazole or its derivative units as acceptors, have been characterized through linear absorbance and fluorescence measurements, nonlinear absorbance, cyclic voltammetry, and differential pulse voltammetry to demonstrate the evolution of narrow HOMO−LUMO gaps ranging from 1.05 to 1.95 eV, with the oligomers composed of EDOT and benzo[1,2-c,3,4-c′]bis[1,2,5]thiadiazole (BBT) exhibiting the narrowest gap. The absorption maxima ranges from 517 to 846 nm and the fluorescence maxima ranges from 651 to 1088 nm for the different oligomers. *Z*-scan and two-photon fluorescence were used to measure the frequency degenerate 2PA of the different oligomers. The oligomer's 2PA cross sections ranged from 900−3500 GM, with the oligomer containing EDOT donor units and a BBT acceptor unit exhibiting the largest 2PA cross section. The use of these oligomers in red to near-IR emitting polymer light-emitting diodes (PLEDs) was demonstrated by blending the soluble emitting oligomers into a suitable host matrix. Energy transfer from the matrix to the emitting oligomer can be achieved, resulting in PLEDs with pure oligomer emission.

KEYWORDS: near-infrared emission, PLED, two-photon absorption, donor−acceptor oligomers, controlled HOMO−LUMO gap

INTRODUCTION

Conjugated polymers have received a great deal of attention because of their applications in photovoltaic devices, light-emitting diodes (LEDs), field-effect transistors (FET), and electrochromic devices.[1−5] Similarly, conjugated oligomers[6] share many of the properties of conjugated polymers with certain advantages including their well-defined structure, easier purification, fewer defects, and the possibility to introduce functionalities. As such, the fabrication of solution-processable polymer light-emitting diodes (PLEDs), vapor-deposited organic light-emitting diodes (OLEDs), and FETs constructed using discrete oligomers is not far from commercial realization. Through cross linking, insoluble films of light-emitting and/or charge-transporting polymer networks can be obtained.[7,8] In one approach, we utilized acrylate functionalized discrete π-conjugated oligomers to create photopatterned films,[4] where the charge-transporting conjugated units could be used to fabricate solution-processable electrochromic devices and organic field-effect transistors (OFETs).

In the work reported here, a family of donor−acceptor−donor (DAD) oligomers has been synthesized in an effort to further our understanding of how donor and acceptor moieties and their relative locations effect the linear absorbance and fluorescence properties, the HOMO−LUMO gap, electrochemical properties, and two-photon absorbance (2PA) cross sections. Introducing a functional end group onto these oligomers also provides an opportunity for incorporating the π-conjugated system covalently into a more complex system similar to our previous approach.[4] For many applications, such as OLEDs[9] and photovoltaics,[3] the value of the HOMO−LUMO gap is critical to an optimized device because it determines the color of the emitted light in the LED or the effectiveness with which solar radiation is absorbed in photovoltaic devices. In the DAD approach employed, the combination of an electron-rich donor

Received: February 4, 2011
Revised: July 18, 2011
Published: August 04, 2011

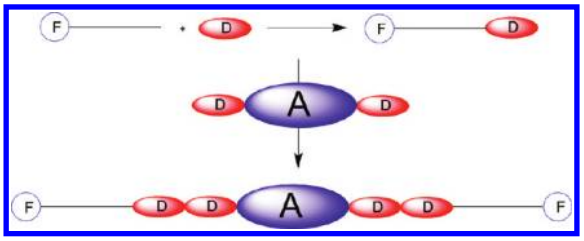

Figure 1. Schematic illustration of the DAD oligomers and the synthetic strategy used to obtain them, where D, A, and F represent donors, acceptors, and functional/protective groups, respectively.

and an electron-deficient acceptor results in a conjugated material with a decreased HOMO−LUMO gap.[10,11] By carefully selecting the appropriate structures of the donor and acceptor, it is possible to tailor the gap and the solubility of the resulting oligomer. One specific donor−acceptor approach to small gap oligomers and polymers is the use of nitrogen-containing heterocycles as effective electron acceptors. For example, small band gaps are reported for electropolymerized donor−acceptor polymers with thiophene or 3,4-ethylendioxythiophene (EDOT) as donors and benzothiadiazole and its derivative units as acceptors.[12−14] In addition to our approach, recent literature describes the use of several different classes of donor−acceptor type molecules such as those consisting of shorter π-conjugated systems containing the same units as reported herein,[15] molecules with triarylamines as electron donors,[16,17] as well as molecules absorbing further into the near-IR such as bis(pyrrolopyrrole) cyanines,[18] and benzene-fused hexaazatriphenylene derivatives[19] among others.

On the basis of similar molecular systems that incorporate π-conjugation in DAD structures and exhibit increased third-order optical nonlinearities,[20−22] the family of oligomers reported here were predicted to display similar and potentially useful nonlinear properties. Materials displaying nonlinear absorbance are expected to have significant impact in optical communications, optical switching, and data storage applications. Furthermore, this DAD oligomer concept lends itself to readily tunable HOMO−LUMO levels, making them potential candidates for materials with controlled 2PA absorbance[20−22] and also controlled emission wavelengths for use in OLEDs or PLEDs.[15−17]

We have focused on developing a series of discrete DAD π-conjugated oligomers[6,12,13] to obtain materials with large 2PA and near-infrared (near-IR) emission.[11,23] Although 2PA increases with increasing conjugation length, molecules with linear absorptions that extend into the near-IR tend to be less photochemically stable. The use of DADs with various strengths of donors and acceptors that extend the linear and therefore 2PA in the near-IR region that are photochemically stable are of interest for many nonlinear applications. In particular, extending photomolecular responses that extend into the telecommunications bands between 1260 and 1675 nm will allow for new uses of molecular systems in optical switching. Furthermore, the use of donor−acceptor-based oligomers in PLEDs and OLEDs has previously been demonstrated and provides many advantages over traditional polymer emitters including more readily tunable emission wavelengths, more facile purification, no end-group effects, and the ability for device fabrication through either solution processing or thermal vapor deposition.[15−17]

As illustrated in Figure 1, the DAD oligomer synthetic strategy involves coupling a donor with a protective or functional end group (F) attached to an alkyl chain, followed by further coupling with a DAD core to create a structure consisting of two solubilizing terminal alkyl groups and a π-conjugated DAD core segment. By introducing a protected alcohol at the end of the alkyl spacers, we are able to easily functionalize the π-conjugated oligomers for the possibility of further reactivity.

This strategy has resulted in the design of new DAD-based oligomeric systems with absorption and emission wavelengths extending over a wide range. Through control of the donor and acceptor strength, the linear absorption maxima ranges from 517 to 846 nm and the emission wavelength maxima from 651 to 1088 nm. On the basis of this technique, the DAD oligomers present readily tunable absorbance and emission properties that allow for their potential use in 2PA applications and red to near-IR emitting PLEDs.

RESULTS AND DISCUSSION

Synthesis of Telechelic Donors. In order to establish the fundamental properties of the π-conjugated segments, we synthesized the four donor synthons **2**, **3**, **7**, and **11** as synthetic starting points as depicted in Scheme 1.

The tetrahydropyran (THP)-protected hexanebromide[14] **1** was converted to the alkylated donors **2** and **3**,[4] whereby thiophene and 2,3-dihydrothieno[3,4-b][1,4]dioxine (EDOT) were reacted with butyllithium followed by addition of the protected hexanebromide. These alkylated donors **2** and **3** were converted to stannylated compounds **4** and **5** by reaction with *n*-BuLi and quenching with a halogenated organotin compound in high yields. 1,4-Dibromo-2,5-bis(heptyloxy)benzene was converted to the 1-aryl-4-bromo-2,5-bis(heptyloxy)benzene **6** via Stille coupling[24−26] with the stannylated alkyl-thiophene **4** using stoichiometric imbalance to ensure dominant monoreaction. Subsequent Stille coupling with 2-tributylstannyl-thiophene afforded the monoalkylated bisthieno-bis(heptyloxy)benzene **7** with a large yield. By reaction with *n*-BuLi and addition of trimethyltinchloride, the stannylated compound **8** was obtained. The donor synthon **11** was synthesized by reacting 1-bromo-3,5dimethoxybenzene with tribromoborane to obtain 5-brombenzen-1,3-diol **9**, which was further converted to compound **10** by reacting with THP protected hexanebromide. Stille coupling with 2-tributylstannyl-thiophene afforded the synthon **11** in high yields. The conversion into the stannylated compound **12** was accomplished using the same method as described for **8**.

Synthesis of Telechelic Donor−Acceptor−Donor Oligomers. The synthesis of telechelic oligomers with 2,1,3-bezothiadiazole (BTD) as the acceptor is shown in Scheme 2a−d. Starting with a palladium-catalyzed Stille coupling of the stannylated compound **4** and bis-brominated-thiophene-benzothiadiazole[10,11,27] (T-BTD-T) **13** or the bis-brominated-EDOT-benzothiadiazole[23,27] (E-BTD-E) **14** DAD core, afforded the difunctionalized THP-protected thiophene oligomers **TT-BTD-TT** (**15**) and **TE-BTD-ET** (**16**) in high yields (Scheme 2a). Stille coupling of compound **5** with **13** and **14** resulted in the corresponding difunctionalized THP-protected EDOT oligomers **ET-BTD-TE** (**17**) and **EE-BTD-EE** (**18**) in reasonable yields (Scheme 2b). Deprotection of **15**, **16**, **17**, and **18** were easily achieved under mildly acidic conditions to give the functional oligomers **TT-BTD-TT-diol**, **TE-BTD-ET-diol**, **ET-BTD-TE-diol**, and **EE-BTD-EE-diol** in excellent yields. After deprotecting the terminal hydroxyl group, the solubility of the oligomers in common organic solvents decreased dramatically. To obtain more soluble alcohols for a later functionalization, **TPT-BTD-TPT**

dx.doi.org/10.1021/cm201424a |*Chem. Mater.* 2011, 23, 3805–3817

Scheme 1. Synthesis of Telechelic Donors

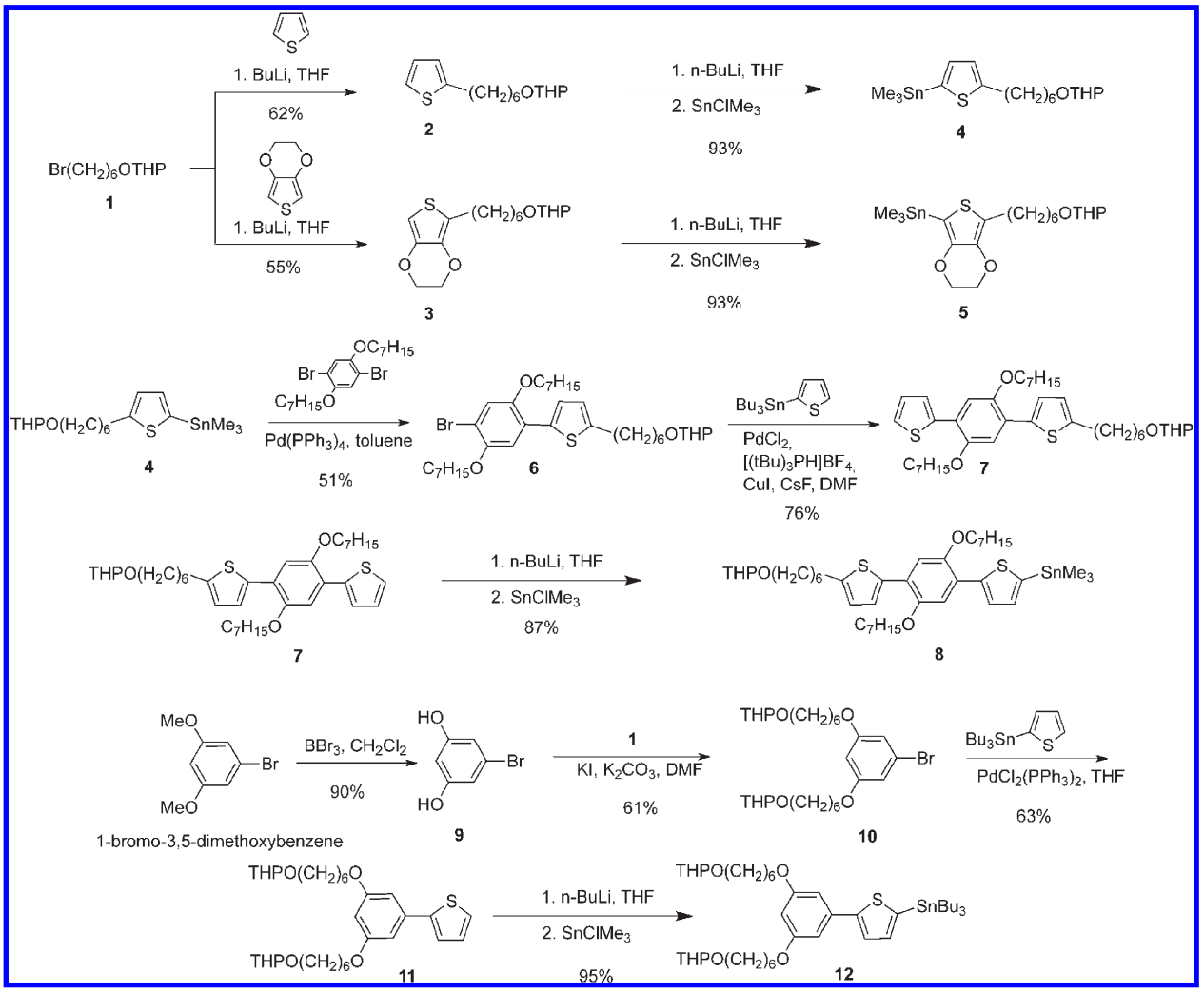

(**19**) was synthesized via the palladium-catalyzed cross coupling of stannyl **8** (TPT) and 4,7-dibromobenzo-[c][1,2,5]thiadiazole (Scheme 2c). Dialkyloxybenzene-thiophene **12** was coupled via Stille coupling to **13** to obtain compound **20** (Scheme 2d). **TPT-BTD-TPT** (**19**) showed a much higher solubility for the alcohol, introduced by the alkoxy-benzene, which was accomplished through mild acidic conditions. The functionalization of the terminal alcohol group, for example into acrylate or ester moieties, is significantly easier according to the increasing solubility of these compounds.

Two thiadiazolo-quinoxaline (TQ) acceptor oligomers were synthesized as described in Scheme 3. Dihexyl-4,9-di(thiophen-2yl)-[1,2,5]thiadiazolo[3,4-*g*]quinoxaline[11] **21** was dibrominated by **22** and then successfully converted to the **TT-TQ-TT** (**23**) by reaction with the THP-protected stannylated compound **4**. By Stille coupling with the THP-protected 2,3-dihydrothieno[3,4-b][1,4] dioxin-5-yl)-stannane **5**, **ET-TQ-TE** (**24**) could be obtained in good yields. Deprotection under mild acidic conditions yielded **TT-TQ-TT-diol** and **ET-TQ-TE-diol**.

Oligomers with benzo[1,2-*c*;4,5-*c*′]bis[1,2,5]thiadiazole (BBT) as the acceptor[28] were synthesized as described in Scheme 4. Therein, 4,8-bis(2,3-dihydrothieno[3,4-*b*][1,4]dioxin-5-yl)benzo-[1,2-*c*;4,5-*c*′]bis[1,2,5]-thiadiazole **25** was brominated with NBS to obtain dibrominated compound **26**. Stille coupling with either **4** or **5** afforded the difunctionalized THP-protected oligomers **TE-BBT-ET** (**27**) and **EE-BBT-EE** (**28**). Deprotection of **26** and **27** was achieved under mildly acidic conditions to give the functional oligomers **TE-BBT-ET-diol** and **EE-BBT-EE-diol** in high yields.

All oligomers were characterized by ^{1}H and ^{13}C NMR spectroscopy and showed narrow and well-defined signals as expected for monodisperse samples; identity and purity were confirmed by EA and HRMS (see Supporting Information for details). Furthermore, the compounds show relatively good thermal stability; only 5% degradation is observed in all cases up to 330 °C. A summary of the synthesized oligomers for ease of reference is presented in Scheme 5.

Optical Spectroscopy. The difference in the donor−acceptor properties of the BTD oligomers is reflected in their photophysical properties as they show two absorbance bands in solution: a high energy band between 320 and 360 nm (3.88−3.44 eV) followed by a low energy band between 517 and 585 nm (2.40−2.12 eV) likely arising from the $\pi-\pi^*$ transition and charge−transfer transition, respectively. All of the oligomers show extinction coefficients between 2×10^4 and 4×10^4 $M^{-1}cm^{-1}$ (Table 1). Importantly, the relative strengths of the

dx.doi.org/10.1021/cm201424a |*Chem. Mater.* 2011, 23, 3805–3817

Scheme 2. (A) Synthesis of BTD-Containing Oligomers (TT-BTD-TT and TE-BTD-ET). (B) Synthesis of BTD-Containing Oligomers (ET-BTD-TE and EE-BTD-EE). (C) Synthesis of Extended BTD Oligomer (TPT-BTD-TPT). (D) Synthesis of Extended BTD Oligomer (PTT-BTD-TTP).

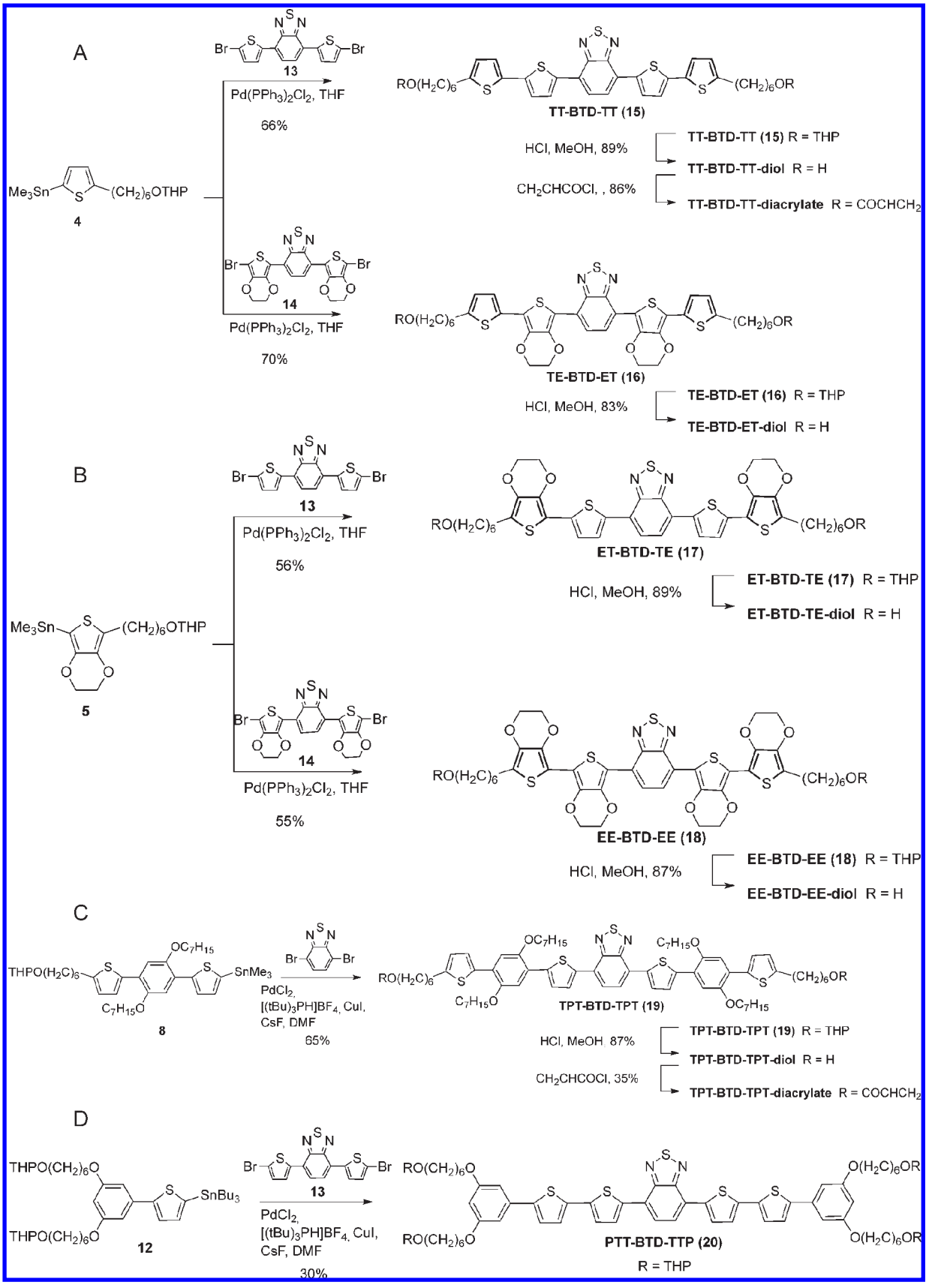

dx.doi.org/10.1021/cm201424a |*Chem. Mater.* 2011, 23, 3805–3817

Scheme 3. Synthesis of Thiadiazolo−Quinoxaline-Containing Oligomers (TT-TQ-TT) and (ET-TQ-TE)

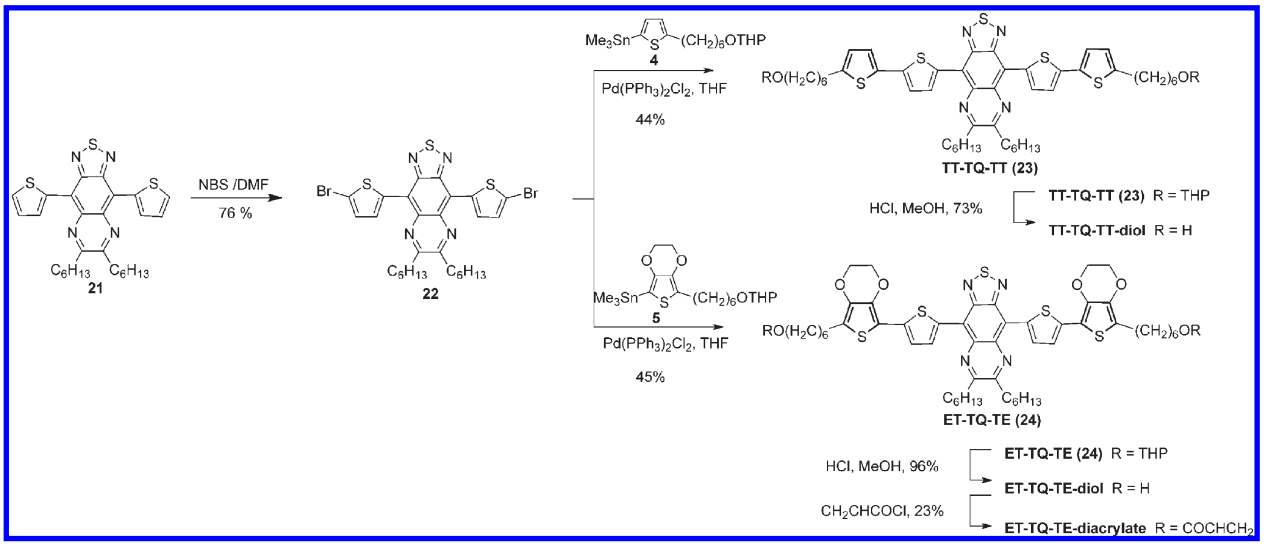

Scheme 4. Synthesis of Benzo[1,2-*c*;4,5-*c*′]bis[1,2,5]thiadiazole-Containing Oligomers (TE-BBT-ET and EE-BBT-EE)

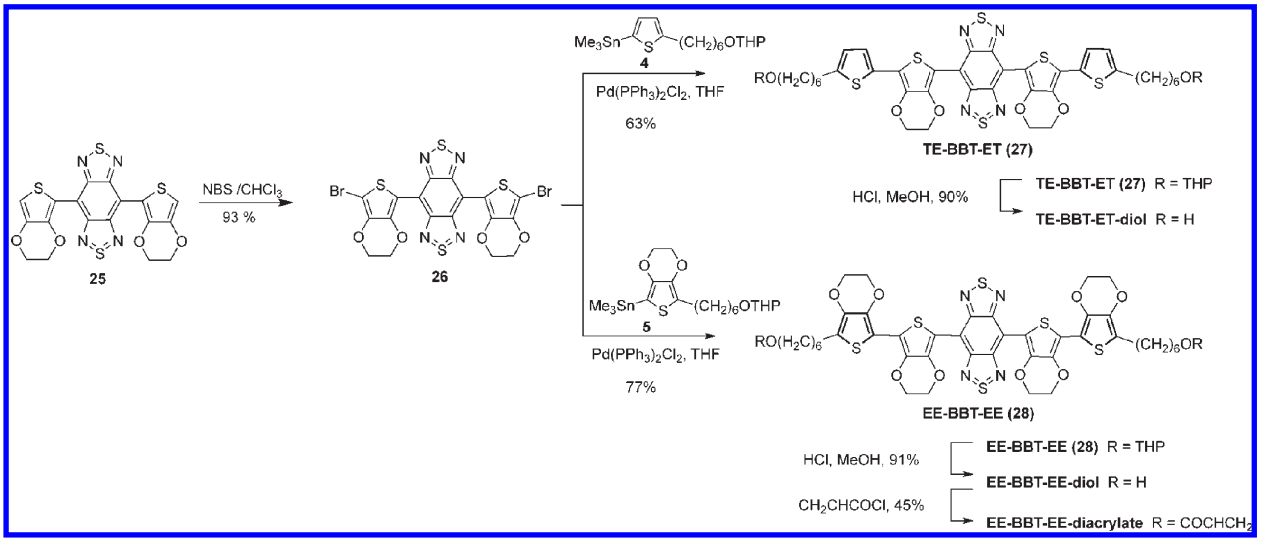

electron donor and acceptor moieties, as well as the length of the conjugated system, are observed to have a large influence on the spectral characteristics of the oligomers and allow us to effectively tune the absorption and emission wavelengths of the systems. In the DAD structures studied here, their linear absorption and emission spectra are characterized by broad spectra with large Stokes shifts in the emission spectra of ∼2000−4500 cm^{-1}. The relatively large Stokes shifts exhibited are common to π-conjugated donor−acceptor compounds and are attributed to a degree of charge−transfer character.[29−31]

Because of the stronger π-donor properties of the EDOT (E) unit in comparison with thiophene (T), panels (a) and (b) of Figure 2 show that changing the outer donor heterocycle in **TT-BTD-TT** into an EDOT donor in **ET-BTD-TE** leads to an absorbance maxima red shift of 30−546 nm, and the solution color changes from red to purple.[10,11] A similar effect is obtained when the position of the thiophene and EDOT units are swapped in **TE-BTD-ET**, as illustrated by the results in panel (c) of Figure 2, where there is a slightly larger DA interaction as the λ_{max} moves to 564 nm. When the stronger EDOT donor is exclusively used in **EE-BTD-EE** (Figure 2d) there is a further bathochromic shift of ∼20 nm, and the solution color changes from dark violet to blue. The incorporation of a conjugation extending phenyl unit to the **TT-BTD-TT** oligomer results in a further 11 and 16 nm red shift for the **PTT-BTD-TTP** and **TPT-BTD-TPT** oligomers, respectively (Supporting Information). In agreement with the absorbance data, the corresponding fluorescence maxima displayed in Figure 2 show similar spectral shifts with emission maxima ranging from 651 nm for **TT-BTD-TT** up to 725 nm for **EE-BTD-EE**.

A similar red shift in both the absorbance and fluorescence spectra is observed when the strength of the electron acceptor is increased. Substitution of BTD with the stronger electron accepting thiadiazolo-quinoxaline (TQ) shifts the DA absorption peak into the near-IR with a maximum of 708 nm for **TT-TQ-TT** and 755 nm for **ET-TQ-TE** as shown in Figure 3. This bathochromic

dx.doi.org/10.1021/cm201424a |*Chem. Mater.* 2011, 23, 3805–3817

Scheme 5. Chemical Structures and Acronyms for the Complete Family of DAD Oligomers

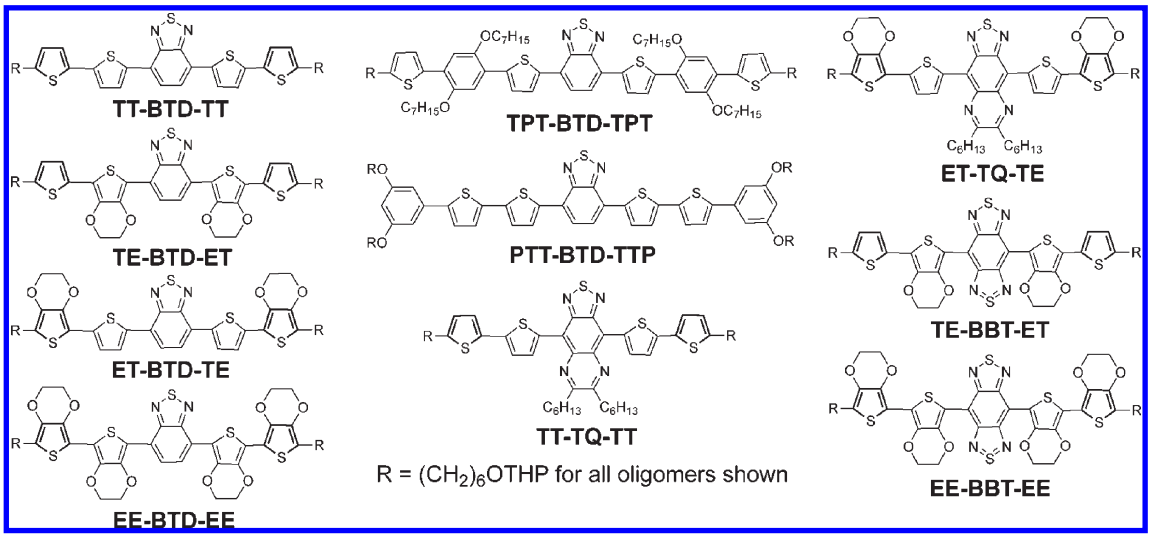

Table 1. Linear and Nonlinear Optical Properties for THP-Protected Oligomer Derivatives

	$\lambda_{max\ ab}$ (nm)[a,b]	ε_{max} ($M^{-1}cm^{-1}$)[a,b,c] ($\times 10^4$)	$\lambda_{max\ em}$ (nm)[a]	Φ_F[c]	μ_{ge} (D)[a]	δ^{max} (GM)[f],	photodecomposition threshold (nJ)[a,g]	Stokes shift (cm^{-1})[a]
TT-BTD-TT	364, 517	3.0	651	0.85[d]	6.7	2500	>100	3981
ET-BTD-TE	377, 546	2.7	686	0.33[d]	6.8	_	10	3738
TE-BTD-ET	388, 564	3.0	692	0.24[d]	6.9	_	10	3279
EE-BTD-EE	396, 585	2.2	725	0.07[d]	6.4	_	10	3300
TPT-BTD-TPT	389, 533	3.3	690	0.40[d]	7.4	2500	>100	4269
PTT-BTD-TTP	390, 528	4.2	676	0.44[d]	8.3	2500	>100	4146
TT-TQ-TT	389, 708	2.1	900	0.03[e]	6.7	900	>100	3073
ET-TQ-TE	404, 755	2.4	974	0.01[e]	7.1	_	40	2978
TE-BBT-ET	391, 786	2.1	1020	0.01[e]	6.3	1600	>100	2919
EE-BBT-EE	359, 404, 846	2.7	1088	0.005[e]	7.3	3500	>100	2629

[a] Measurements performed in $CHCl_3$. [b] All measurements performed with a Varian Cary 500 Scan UV−vis-near-IR spectrophotometer at the University of Florida. [c] Estimated error in ε_{max} and Φ_F values is ±10%; Φ_F values measured in $CHCl_3$ or toluene as noted. [d] Standard: Rhodamine B in EtOH (Φ_F = 0.65),[38] excitation wavelength 510 nm, oligomer fluorescence measured in $CHCl_3$. [e] Standard: H_2TPTBP in toluene (Φ_F = 0.03),[39] excitation wavelength 430 nm, oligomer fluorescence measured in toluene due to poor stability of H_2TPTBP standard in $CHCl_3$. [f] **ET-BTD-TE**, **TE-BTD-ET**, **EE-BTD-EE**, and **ET-TQ-TE** have low optical damage thresholds, which do not enable 2PA measurement. [g] Damage threshold energies correspond to 140 fs (fwhm) pulse widths focused to a spot size of ~20 μm (HW/e^2) in $CHCl_3$. Error bars are typically 15−20%. Of the oligomers that showed photodecomposition thresholds <100 nJ, the thresholds are reported at wavelengths of 820 nm for **TE-BTD-ET** and **ET-BTD-TE**, 740 nm for **EE-BTD-EE**, and 1140 nm for **ET-TQ-TE**.

shift of the low energy peak, with little change in the high energy peak, leads to a green color of the solution as a window of transmission opens up in the middle of the visible spectrum at 532 nm, which may be useful for excited state absorption applications.[27,32−34] The fluorescence of the two TQ compounds are completely shifted to the near-IR region, with emission maxima of 900 nm for **TT-TQ-TT** and 974 nm for **ET-TQ-TE**. By replacing the TQ acceptor with bisbenzothiadiazole (BBT), the strongest acceptor of the BTD derivatives, an additional bathochromic shift to the near-IR is observed due to the more intense donor−acceptor interaction as illustrated by the spectral data for **TE-BBT-ET** and **EE-BBT-EE** in Figure 4.[10,11] When the external thiophene donor (**4**) is coupled to the E-BBT-E core, an absorption maximum of 786 nm is observed, while the stronger donor EDOT (**5**) yields a further bathochromic shift to 847 nm. In spite of the large difference in the absorption maxima, both solutions have nearly the same color as the window of transmission in the center of the visible spectrum dominates. As expected from the absorbance data, the fluorescence of these compounds is shifted further into the near-IR with fluorescence maxima at 1020 and 1088 nm for **TE-BBT-ET** and **EE-BBT-EE**, respectively.

All of the THP protected oligomers are highly soluble in a wide range of organic solvents (e.g., toluene, tetrahydrofuran, chloroform), but unfortunately after acidic deprotection the resulting alcohols are only slightly soluble in toluene or chloroform and only show sufficient solubility in THF. This low solubility of the alcohols precluded further chemistry being carried out on these derivatives, and as such, the absorbance and emission spectra reported here and compiled in Table 1 are all for the THP protected oligomers.

Table 1 compiles the fluorescence quantum yields for the series of THP protected oligomers. Interestingly, it is evident that the quantum yield decreases systematically as the fluorescence red shifts (lower energy). This general trend is likely the result of

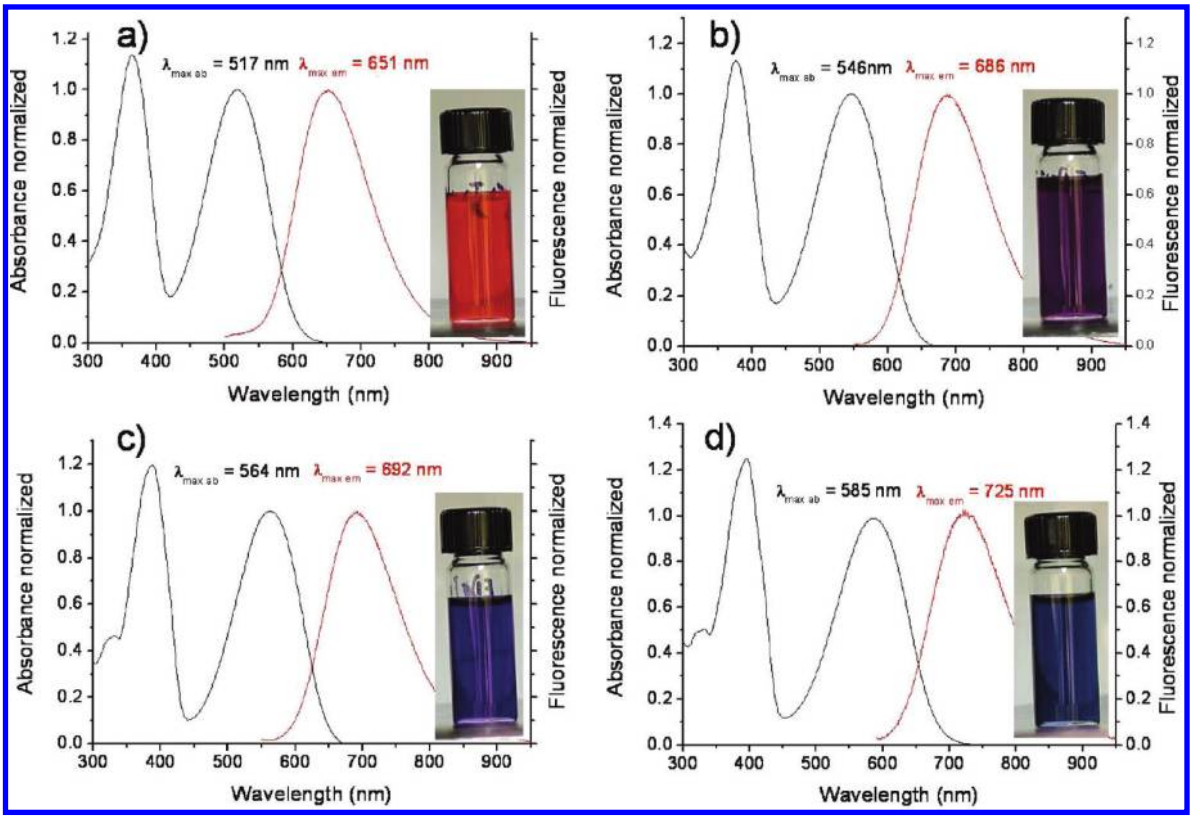

Figure 2. Absorption (black) and emission (red) spectra for THP protected **TT-BTD-TT** (a), **ET-BTD-TE** (b), **TE-BTD-ET** (c), and **EE-BTD-EE** (d) in chloroform solution (C = 50 μM).

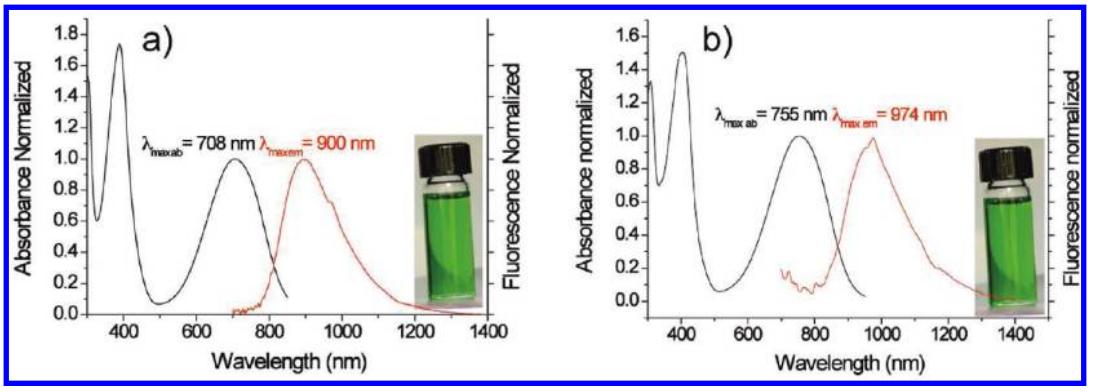

Figure 3. Absorption (black) and emission (red) spectra for THP protected **TT-TQ-TT** (a) and **ET-TQ-TE** (b) in chloroform solution (C = 50 μM).

an increase in the nonradiative decay rate with decreasing excited state energy (energy gap law).[35,36] The quantum yields are highest for the oligomers that emit at λ < 700 nm, with the **TT-BTD-TT** system having the highest yield at ~85%. The oligomers that feature three aryl rings flanking the acceptor unit (**TPT-BTD-TPT** and **PTT-BTD-TTP**) have comparatively high yields. This effect may be due to an increase in the radiative rate resulting from the longer conjugation length in the three ring systems. The fluorescence yields are substantially lower for the systems that emit at λ > 700 nm, with yields ~1% or less for the systems that emit at 1 μm or longer. While these yields are relatively low, they are comparable with other organic dyes that emit at comparable wavelengths in the near-IR region.[16,37]

The frequency degenerate 2PA spectroscopy for the samples in Table 1 was performed with two different experimental techniques, Z-scan[40,41] and two-photon fluorescence (2PF).[42] For all these samples, the fluorescence spectra extend beyond the range of the 2PF detection system, and thus, the 2PF method does not provide an absolutely calibrated measurement of the 2PA cross section. Instead, open-aperture Z-scans were used to absolutely calibrate the values for the 2PA cross section, δ_{2PA}. All compounds were prepared in chloroform for the nonlinear optical characterization

Figure 5 shows the linear and 2PA spectra for the measurable BTD acceptor samples with three different donor groups; TT, TPT, and PTT. It should be noted that the molar absorptivity values differ slightly (≤10%) from ε_{max} as listed in Table 1. This is

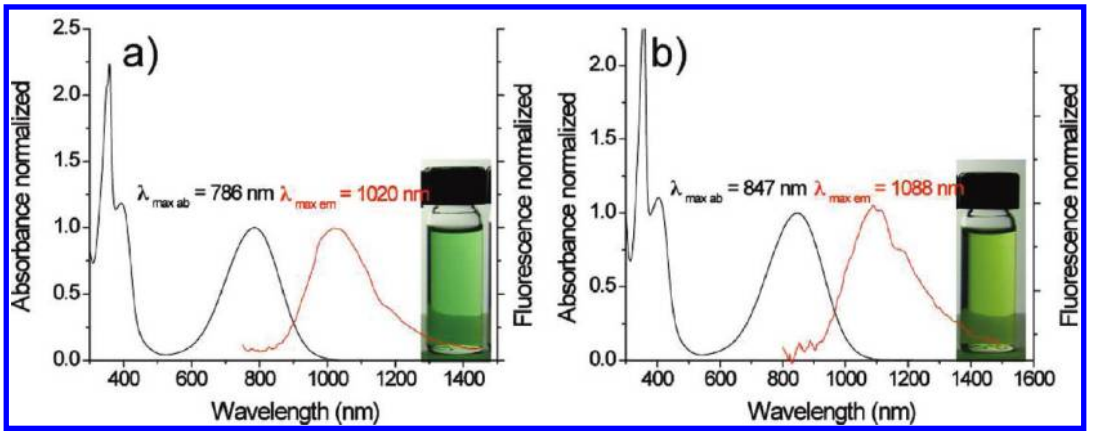

Figure 4. Absorption (black) and emission (red) spectra for THP protected **TE-BBT-ET** (a) and **EE-BBT-EE** (b) in chloroform solution ($C = 50\,\mu M$).

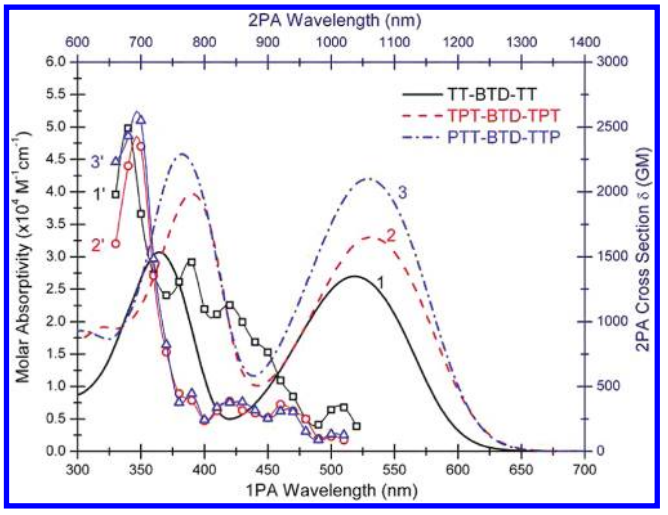

Figure 5. Molar absorptivity (1,2,3) and 2PA measured with 2 photon fluorescence and scaled with *Z*-scan (1′,2′,3′) for BTD acceptors with TT, TPT, and PTT donors in chloroform, respectively. Molar absorptivity measurements performed with a Varian Cary 500 Scan UV−vis-near-IR spectrophotometer at the University of Central Florida.

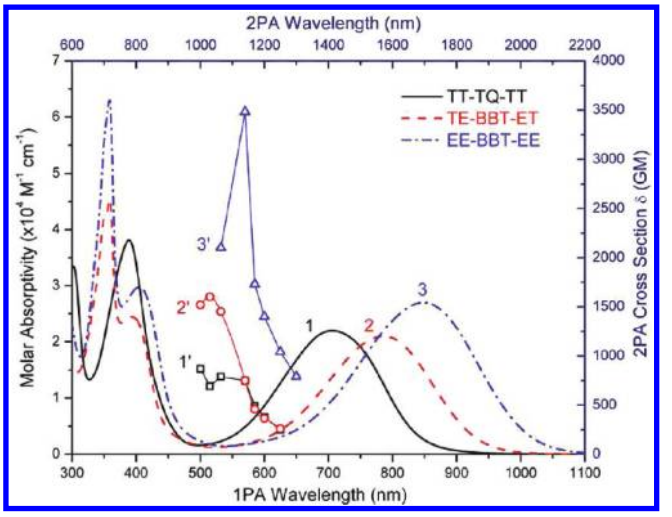

Figure 6. Molar absorptivity (1,2,3) and 2PA measured with *Z*-scan (1′,2′,3′) for the TQ acceptor and BBT acceptors with TE and EE donor groups, respectively. Molar absorptivity measurements performed with a Varian Cary 500 Scan UV−vis-near-IR spectrophotometer at the University of Central Florida.

due to the measurements being performed at two different universities and potential discrepancies in the calibration of the balances used in weighing the samples and/or the calibration of the UV−vis-near-IR. All measurements included in Table 1 were measured on the same instrument, and all values reported in Figures 5 and 6 were measured on the same model instrument at another university, thereby allowing direct comparisons within the respective data sets. One of many factors influencing 2PA is the transition dipole moment from the ground to first excited state, μ_{ge}. A large μ_{ge} leads to an enhancement of 2PA because the first excited state is considered the intermediate state in this 2PA transition.[43,44] The transition dipole moment μ_{ge} can be calculated (results shown in Table 1) from the integrated strength of the lowest energy band in the linear absorption spectrum by[45−47]

$$\mu_{ge} = \sqrt{\frac{1500(\hbar c)^2 \ln 10}{\pi N_A E_{ge}} \int \varepsilon_{ge}(\nu)\mathrm{d}\nu}$$

where N_A is Avogadro's number (6.022×10^{23}), $\varepsilon_{ge}(\nu)$ is the extinction coefficient in $cm^{-1}\,M^{-1}$ at the wavenumber υ, in cm^{-1}, and the integration is over the main absorption band (all parameters are in CGS units). For the BTD acceptor series (Figure 5), transition dipole moments increase slightly with donor strength as shown in Table 1, but no significant changes are observed in either the magnitude or peak spectral positions of the 2PA spectra. Because of the symmetry of the molecules, 2PA underneath the main absorption band are expected to be small with contributions arising from symmetry breaking and possibly a low-lying electronic transition. Although symmetry breaking appears to be the most reasonable explanation, quantum chemical calculations would be necessary to provide a more direct conclusion. The 2PA cross sections of 2500 GM with maxima near 700 nm are comparable to other conjugated molecules with 2PA in this wavelength range.[20−22]

Shown in Figure 6 are the linear and 2PA spectra for the molecules containing the stronger acceptors, TQ and BBT indicating a significant red shift from the BTD acceptors. Comparing the linear absorption of **TT-BTD-TT** from Figure 5 and **TT-TQ-TT** from Figure 6 (identical donors), yields a red shift by ∼200 nm, presumably due to the influence of the

dx.doi.org/10.1021/cm201424a |*Chem. Mater.* 2011, 23, 3805–3817

stronger acceptor TQ as previously discussed. Unfortunately, a comparison can not be made between the two TQ containing oligomers because of the photoinstability of the **ET-TQ-TE** derivative. Combining the strongest acceptor in the series (BBT) with the strongest donor group (EE) shows an additional red shift in the linear absorption spectrum, a larger transition dipole moment, and the largest measured 2PA cross section of all the samples, being nearly twice as large as the TE donor group associated with the BBT acceptor.

It is well-known that increasing the length of conjugation typically red shifts the main linear absorption band and increases 2PA in several types of conjugated systems.[48,49] In acceptor modified cyanines and thiophene-based systems, increasing the strength of the donor and/or acceptor also enhances 2PA cross sections.[50] In accordance with these previous reports, an increase in 2PA cross sections is observed for the stronger donors (EE vs TE) in the BBT system; however, no increase is observed for the derivatives based on the weaker BTD acceptor. Recently, a series of modified donor groups has been shown to significantly red shift the linear absorption band by extending the conjugation further into the end groups.[51] This effective lengthening of the conjugated system may also be a possible explanation for the red shift observed when the donor and/or acceptor strength is increased in this oligomer family.

Z-scan measurements suggest that the presence of one or more pair of EDOT donors on the BTD and TQ oligomers reduces the photochemical stability of the molecule because photoinduced decomposition was observed when **ET-BTD-TE**, **TE-BTD-ET**, and **EE-BTD-EE** were pumped with as little as 10 nJ per pulse, an energy much smaller than that needed to observe any 2PA. Photodecomposition thresholds for **ET-TQ-TE** were also observed but at larger input energies (~40 nJ) as shown in Table 1. These energies are for 140 fs (fwhm) pulse widths focused to a spot size of ~20 μm (HW/e^2 M).

Electrochemistry. Electrochemical methods provide a means of establishing the HOMO and the LUMO energies of conjugated systems. These values are critical for selecting the appropriate cathode and anode materials in an LED or photovoltaic device, selecting an appropriate host polymer in a PLED, and for selecting the appropriate complementary donor−acceptor in a photovoltaic device.[52] Although **TT-BTD-TT**[53] has been published previously, no electrochemical data have been reported on the alkylated oligomers. Here, we attempted a variety of techniques to establish the redox properties of all THP-protected BTD, TQ, and BBT-oligomers. Cyclic voltammetry (CV) in CH_2Cl_2 solution yielded reproducible redox processes between 0.6 V and −1.9 V versus Fc/Fc$^+$ in an oxygen and water-free environment. Also differential pulse voltammetry (DPV) behavior of all THP protected oligomers was obtained as DPV offers better sensitivities than CV and leads to steeper peak onsets due to the sharper current response occurring near the E^o region. The peak shapes seen in DPV also allude to the redox behavior of the system. True reversible systems exhibit sharper, more well-defined peaks, while quasi-reversible and irreversible systems give broad peaks.[54]

The two following equations are used to estimate the HOMO and LUMO levels.[52,55]

$$E_a(E_{LUMO}) = -(E_{1/2red} + 5.1)eV$$

$$I_p(E_{HOMO}) = -(E_{1/2ox} + 5.1)eV$$

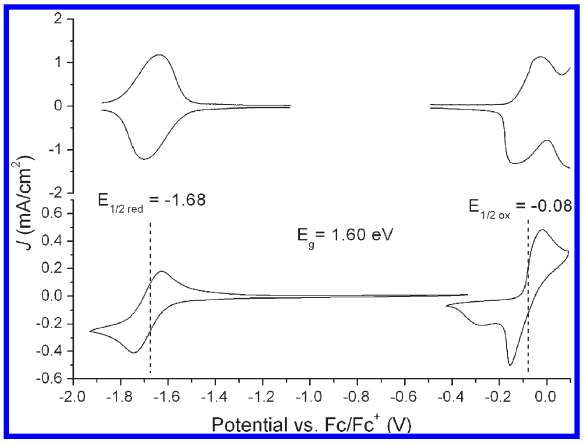

Figure 7. Cyclic voltammetry (bottom) at 50 mV s^{-1} and differential pulse voltammetry (top) with a step time of 0.1 s and a step size of 2 mV for **EE-BTD-EE** (4 mM) in CH_2Cl_2/TBAP (0.1 M) solution.

where $E_{1/2\ red}$ and $E_{1/2\ ox}$ are the half-wave potential measured for the compounds in solution versus the Fc/Fc$^+$ reference. The electrochemically determined HOMO−LUMO gaps were then compared with the optical gap.[56] All optical HOMO−LUMO gaps were taken as the intersection of the fluorescence and absorbance spectra.

The oxidation and the reduction processes recorded by DPV, for example oligomer **EE-BTD-EE** as shown in Figure 7, have sharper onsets than those associated with cyclic voltammetry (See CV and DPV data of all oligomers in the Supporting Information). The $E_{1/2}$ of oxidation and reduction for **EE-BTD-EE** are −0.08 V and −1.68 V, respectively, leading to an estimated HOMO−LUMO gap of 1.60 eV. The optical HOMO−LUMO gap for the neutral oligomer determined by the intersection of the absorbance and fluorescence spectra appeared to be 1.89 eV, which is 0.29 eV greater than the electrochemical gap. Using the electrochemical results, we are able to estimate the HOMO value at −5.02 eV and the LUMO value at −3.42 eV for **EE-BTD-EE**. The electrochemical results for all oligomers are summarized in Table 2, along with their estimated HOMO and LUMO levels. Cyclic voltammetry of **ET-TQ-TE** (Figure 8) shows an $E_{1/2}$ of 0.27 V for oxidation and two reductions with $E_{1/2}$ at −0.94 and −1.45 V, respectively.[28] To the best of our knowledge, this is the first report of an oligomer containing the [1,2,5]thiadiazolo[3,4-*g*]quinoxaline acceptor showing two reversible reductions. Two reversible reductions are also obtained for the **TT-TQ-TT**, **TE-BBT-ET** and **EE-BBT-EE** oligomers (Supporting Information).

For all oligomers in this paper, there is a good correlation between the donor−acceptor interaction strength and the decreasing of the HOMO−LUMO gap. This may allow us to more accurately predict HOMO and LUMO gaps for unknown compounds using the same or similar donor−acceptor units.

Near-IR PLEDs. Polymer-based light-emitting devices (PLEDs) with near-IR emission were fabricated through doping the near-IR emitting THP-protected oligomer, **EE-BTD-EE**, into a conducting polymer matrix selected such that energy transfer from the matrix to the oligomer occurred. The two host matrices used were MEH-PPV and a blend of PVK with PDB (6:4 by weight, where PVK = poly(N-vinylcarbazole) and PBD = 2-(4-biphenyl)-5-(4-tert-butylphenyl)-1,3,4-oxadiazole). Through host to oligomer energy transfer, both host matrices resulted in nearly pure **EE-BTD-EE** emission. Figure 9

Table 2. Summarized Electrochemical Properties of the THP-Protected Oligomers[a]

oligomer	$E_{1/2\ ox}$[b] (V)	$E_{1/2\ red}$[b] (V)	HOMO (eV)	LUMO (eV)	HOMO−LUMO Gap_{ec} (eV)	HOMO−LUMO Gap_{opt} (eV)
TT-BTD-TT	0.49	−1.46	−5.5	−3.64	1.95	2.13
PTT-BTD-TTP	0.33	−1.51	−5.43	−3.59	1.84	2.04
TPT-BTD-TPT	0.30	−1.40	−5.40	−3.70	1.70	2.04
ET-BTD-TE	0.14	−1.68	−5.24	−3.42	1.82	2.00
TE-BTD-ET	0.14	−1.61	−5.24	−3.49	1.75	1.98
EE-BTD-EE	−0.08	−1.68	−5.02	−3.42	1.60	1.89
TT-TQ-TT	0.23	−1.19, −1.69	−5.33	−3.91	1.42	1.52
ET-TQ-TE	0.27	−0.94, −1.45	−5.37	−4.16	1.21	1.43
TE-BBT-ET	0.29	−0.93, −1.59	−5.39	−4.17	1.22	1.37
EE-BBT-EE	0.09	−0.96, −1.63	−5.19	−4.14	1.05	1.28

[a] Note, $E_{1/2\ ox}$ and $E_{1/2\ red}$ were measured in CH_2Cl_2/TBAP, and HOMO-LUMO Gap_{opt} was measured in $CHCl_3$. [b] All measurements done in CH_2Cl_2 and are reported vs Fc/Fc^+.

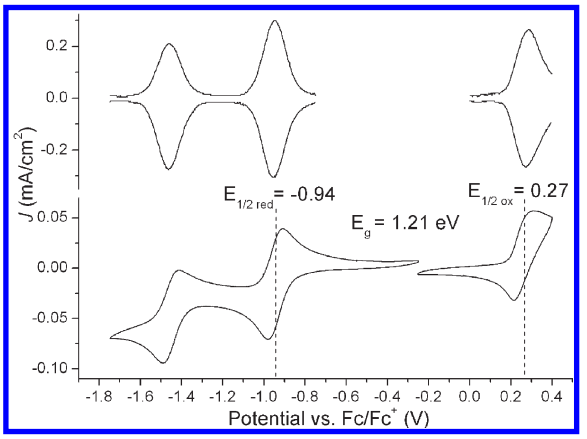

Figure 8. Cyclic voltammetry (bottom) at 50 mV $s^{-1}$and differential pulse voltammetry (top) with a step time of 0.1 s and a step size of 2 mV for **ET-TQ-TE** (4 mM) in CH_2Cl_2/TBAP (0.1 M) solution at 50 mV s^{-1}.

displays the molecules used in the devices and the HOMO−LUMO levels of the two systems.

The energy diagram presented in Figure 9 shows the potential of both PVK:PBD and MEH-PPV to serve as appropriate hosts for the **EE-BTD-EE** oligomer based on a charge trapping mechanism.[57,58] The good spectral overlap of the MEH-PPV emission with the **EE-BTD-EE** absorption suggests that Förster energy transfer from MEH-PPV to **EE-BTD-EE** will occur in addition to charge trapping. Efficient energy transfer from host to **EE-BTD-EE** was observed to occur for both systems, resulting in primarily **EE-BTD-EE** emission in the PLEDs as evident in Figures 10 and 11.

The MEH-PPV blend device shown in Figure 10 shows incomplete energy transfer from MEH-PPV to **EE-BTD-EE** at low doping levels and a significant decrease in emission intensity with increasing **EE-BTD-EE** concentration. Additionally, the **EE-BTD-EE** emission maximum shows a bathochromic shift with increasing concentration. This combination of emission quenching and a bathochromic shift with increasing oligomer concentration are characteristics of aggregation.

The PVK:PBD blend device shown in Figure 11 shows much more complete energy transfer to **EE-BTD-EE** at low concentrations with no PVK emission evident for the 1% device even at larger voltages as displayed in panel (b) of Figure 11. The same quenching effects with increasing **EE-BTD-EE** concentration as

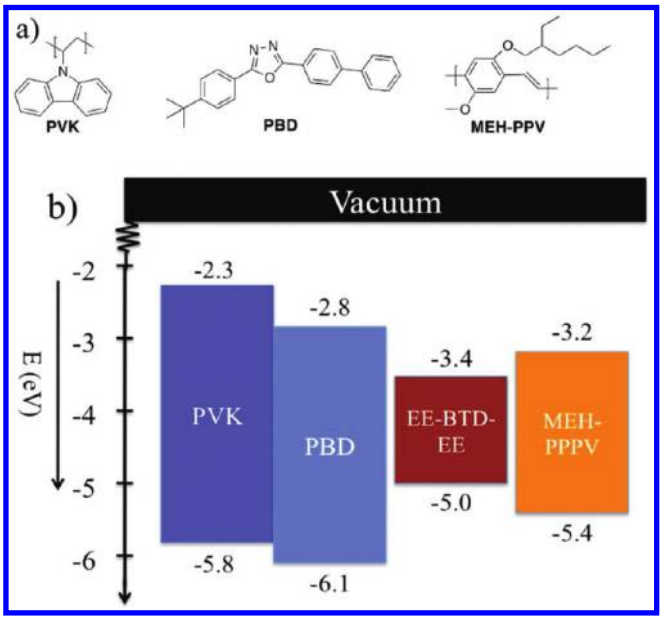

Figure 9. Structures of the molecules used in the near-IR emitting PLEDs (a) and an energy diagram showing HOMO and LUMO levels of PVK,[57] PBD,[57] MEH-PPV,[52] and **EE-BTD-EE**. PVK, PBD, and MEH-PPV HOMO and LUMO values were taken from the literature and calculated with Fc/Fc^+ at −5.1 eV vs vacuum.[52]

observed for the MEH-PPV devices are also observed for the PVK:PBD devices, suggesting that the **EE-BTD-EE** oligomer has a strong tendency to aggregate regardless of the host matrix. The radiant emittance of the **EE-BTD-EE** in MEH-PPV PLEDs was measured and further supports the aggregation quenching evident in the spectral measurements as shown in Figure 12.

The maximum radiant emittance of the devices decreased from 4.5 to 3.1 to 1.3 mW/cm^2 as the concentration of **EE-BTD-EE** in MEH-PPV was increased from 0 to 2 to 4%, respectively. Additionally, the EQE showed a similar trend as it decreased from 0.87 to 0.28% as the concentration of **EE-BTD-EE** was increased from 0 to 4%. This decreased radiance emittance and efficiency with increasing oligomer concentration again indicates that aggregation is occurring and negatively affecting the device performance.

AFM and TEM measurements were performed on the films to probe their morphology. These results, as displayed in Figure 13,

dx.doi.org/10.1021/cm201424a |*Chem. Mater.* 2011, 23, 3805–3817

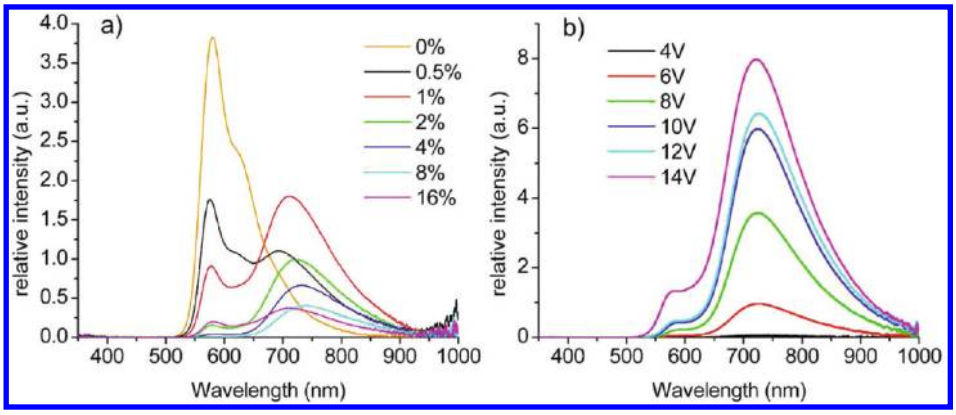

Figure 10. Electroluminescence spectra of (a) varying percent (by wt) **EE-BTD-EE** in MEH-PPV at 6 V and (b) electroluminescence spectra of an optimized 2% **EE-BTD-EE** in MEH-PPV device as a function of applied voltage.

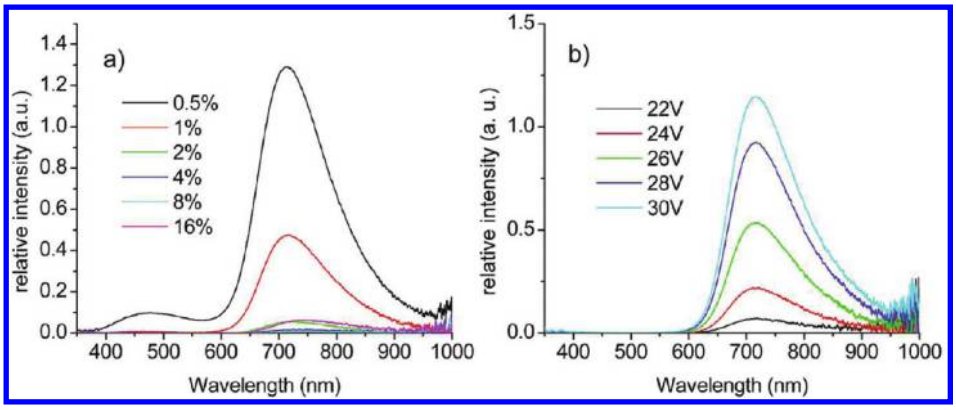

Figure 11. Electroluminescence spectra of varying percent (by wt) **EE-BTD-EE** in PVK:PBD at 26 V (a) and electroluminescence spectra of an optimized 1% **EE-BTD-EE** in PVK:PBD device as a function of applied voltage (b).

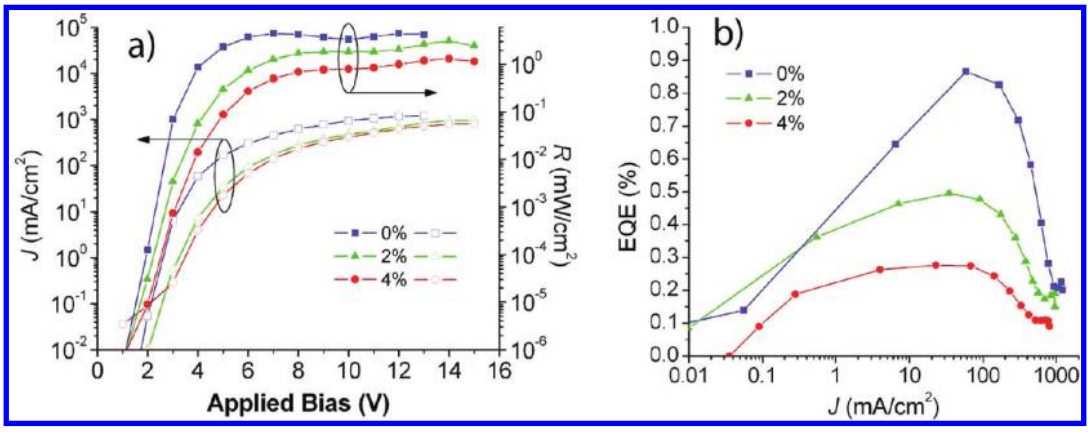

Figure 12. Current density (open symbols) and radiant emittance (filled symbols) for varying percent (by wt) **EE-BTD-EE** in MEH-PPV (a) and percent external quantum efficiencies (EQEs) for the same devices (b).

suggest the presence of aggregates as the concentration of **EE-BTD-EE** in MEH-PPV is increased from 4% to 16%. The evolution of aggregate formation is apparent in the AFM and TEM images as the 4%, 8%, and 16% devices show a dramatic increase in the number of aggregates and a changing morphology. Additional morphological information was obtained through AFM phase imaging, and for the 4% and 8% devices an underlying morphology that is not apparent in the corresponding height images is observed. The TEM images confirm the presence of the aggregates observed in the AFM images. Multiple TEM and AFM images confirmed that the morphology is uniform throughout the films in the case of the 2%, 4%, and 8% blend devices; however, the 16% device showed evidence of two different morphologies.

The AFM and TEM images presented in Figure 13 display the dominant morphology of the 16% blend device. This aggregation

dx.doi.org/10.1021/cm201424a |*Chem. Mater.* 2011, 23, 3805–3817

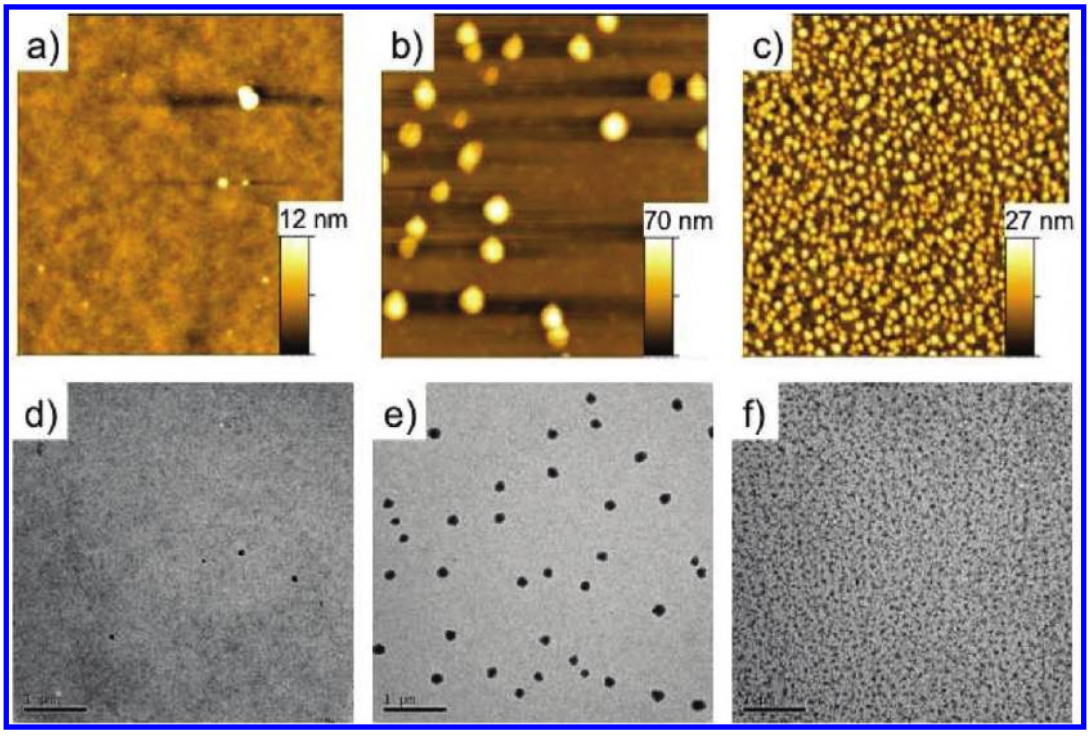

Figure 13. AFM height images of 4%, 8%, and 16% (a−c, respectively) **EE-BTD-EE** in MEH-PPV and the corresponding TEM images (d−f). AFM images are all 5 μm × 5 μm. TEM scale bar is 1 μm.

apparent in all images is attributed to the polar nature of the DAD oligomer and the rod-like extended π-conjugated core with solubilizing groups present only on the ends. These oligomer−oligomer interactions in combination with the less-polar polymer host matrix lead to phase separation and aggregation of the oligomer.

The formation of larger aggregates visible through AFM and TEM suggest that the **EE-BTD-EE** oligomer has a strong tendency to aggregate. Given this tendency to aggregate, it is likely that smaller aggregates not visible through TEM or AFM are also present in the film. These smaller aggregates likely contribute significantly to the decreased device performance observed upon increasing oligomer concentration. This is supported by the ∼50% decrease in device performance of the 4% **EE-BTD-EE** device vs the 2% **EE-BTD-EE** device, even though minimal aggregates are observed in the 4% device.

CONCLUSIONS

A series of oligomers composed of aromatic donor and *o*-quinoid-acceptor units was prepared. The electronic spectra and the color of these oligomers were greatly affected by the properties of the thiophene, phenylene, or 3,4-ethylendioxythiophene donors and by benzothiadiazole or its derivative heterocycles as acceptors. By introducing terminal alkyl chains end capped with a protected alcohol group, a later functionalization can be achieved.[4] The electrochemical behavior of the oligomers show HOMO−LUMO gaps in the range of 1.05−1.95 eV, mainly depending upon the properties of the *o*-quinoid-acceptor heterocycle. Nonlinear 2PA cross sections have been determined to be in the range of 900−3500 GM for the different oligomers and dependent on the donor and acceptor strengths. Owing to the solution processability, the oligomers can be easily integrated into PLEDs as the emitting species using soluble host polymers. Specifically, the near-IR emitting oligomer **EE-BTD-EE** was blended into a charge transporting matrix, and through energy transfer processes, PLEDs with solely oligomer emission were created. On the basis of the oligomers presented in this paper, PLEDs with emission maxima ranging from 651 to 1088 nm could be fabricated; however, the EQE of the PLEDs would be expected to decrease as the emission is further shifted to the near-IR in accordance with the quantum yields. Additionally, the effects of donor and acceptor interactions presented herein provide a basis for additional wavelength tunability.

ASSOCIATED CONTENT

Supporting Information. Experimental details regarding the synthesis, optical spectroscopy, nonlinear optical spectroscopy, electrochemistry, PLED fabrication and characterization, and morphology characterization; synthetic details, mass spectrometric characterization, and NMR characterization; and cyclic voltammetry and differential pulse voltammetry on all oligomers. This material is available free of charge via the Internet at http://pubs.acs.org.

AUTHOR INFORMATION

Corresponding Author

E-mail: reynolds@chem.ufl.edu. Phone: 352-392-9151. Fax: 352-392-9741.

ACKNOWLEDGMENT

We gratefully acknowledge financial support of the present work by the support of the Office of Naval Research MORPH N00014-06-1-0897. S.E., K.G., R.F., K.S., and J.R. also acknowledge the U.S. Defense Advanced Research Projects Agency

(DARPA) and the U.S. Army Aviation and Missile Research, Development, and Engineering Center (AMRDEC) (Project No. W31P4Q-08-1-0003).[59] L.P., T.E., H.H., S.W., D.H., and E.V.S. also acknowledge financial support from the U.S. Army Research Offices by both W911NF0710232 and 50372-CH-MUR.

REFERENCES

(1) Kono, T.; Kumaki, D.; Nishida, J. I.; Sakanoue, T.; Kakita, M.; Tada, H.; Tokito, S.; Yamashita, Y. *Chem. Mater.* **2007**, *19*, 1218–1220.
(2) Aldakov, D.; Palacios, M. A.; Anzenbacher, P. *Chem. Mater.* **2005**, *17*, 5238–5241.
(3) Dhanabalan, A.; van Duren, J. K. J.; van Hal, P. A.; van Dongen, J. L. J.; Janssen, R. A. J. *Adv. Funct. Mater.* **2001**, *11*, 255–262.
(4) Nielsen, C. B.; Angerhofer, A.; Abboud, K. A.; Reynolds, J. R. *J. Am. Chem. Soc.* **2008**, *130*, 9734–9746.
(5) Beaujuge, P. M.; Ellinger, S.; Reynolds, J. R. *Nat. Mater.* **2008**, *7*, 795–799.
(6) Ellinger, S.; Ziener, U.; Thewalt, U.; Landfester, K.; Moeller, M. *Chem. Mater.* **2007**, *19*, 1070–1075.
(7) Facchetti, A. *Mater. Today* **2007**, *10*, 28–37.
(8) Champion, R. D.; Cheng, K.-F.; Pai, C.-L.; Chen, W.-C.; Jenekhe, S. A. *Macromol. Rapid Commun.* **2005**, *26*, 1835–1840.
(9) Aldred, M.; Carrasco-Orozco, M.; Contoret, A.; Dong, D.; Farrar, S.; Kelly, S.; Kitney, S.; Mathieson, D.; O'Neill, M.; Tsoi, W. C.; Vlachos, P. *Liq. Cryst.* **2006**, *33*, 459–467.
(10) Karikomi, M.; Kitamura, C.; Tanaka, S.; Yamashita, Y. *J. Am. Chem. Soc.* **1995**, *117*, 6791–6792.
(11) Kitamura, C.; Tanaka, S.; Yamashita, Y. *Chem. Mater.* **1996**, *8*, 570–578.
(12) Kitamura, C.; Saito, K.; Nakagawa, M.; Ouchi, M.; Yoneda, A.; Yamashita, Y. *Tetrahedron Lett.* **2002**, *43*, 3373–3376.
(13) Van Mullekom, H. A. M.; Vekemans, J. A. J. M.; Havinga, E. E.; Meijer, E. W. *Mater. Sci. Eng.* **2001**, *32*, 1–40.
(14) Binisti, C.; Assogba, L.; Touboul, E.; Mounier, C.; Huet, J.; Ombetta, J.-E.; Dong, C. Z.; Redeuilh, C.; Heymans, F.; Godfroid, J.-J. *Eur. J. Med. Chem.* **2001**, *36*, 809–828.
(15) Yang, Y. X.; Farley, R. T.; Steckler, T. T.; Eom, S. H.; Reynolds, J. R.; Schanze, K. S.; Xue, J. G. *Appl. Phys. Lett.* **2008**, *93*, 163305.
(16) Qian, G.; Dai, B.; Luo, M.; Yu, D. B.; Zhan, J.; Zhang, Z. Q.; Ma, D. G.; Wang, Z. Y. *Chem. Mater.* **2008**, *20*, 6208–6216.
(17) Qian, G.; Zhong, Z.; Luo, M.; Yu, D. B.; Zhang, Z. Q.; Wang, Z. Y.; Ma, D. G. *Adv. Mater.* **2009**, *21*, 111–116.
(18) Fischer, G. M.; Daltrozzo, E.; Zumbusch, A. *Angew. Chem., Int. Ed.* **2011**, *50*, 1406–1409.
(19) Luo, M.; Shadnia, H.; Qian, G.; Du, X.; Yu, D.; Ma, D.; Wright, J. S.; Wang, Z. Y. *Chem.—Eur. J.* **2009**, *15*, 8902–8908.
(20) Webster, S.; Fu, J.; Padilha, L. A.; Przhonska, O. V.; Hagan, D. J.; Van Stryland, E. W.; Bondar, M. V.; Slominsky, Y. L.; Kachkovski, A. D. *Chem. Phys.* **2008**, *348*, 143–151.
(21) Belfield, K. D.; Bondar, M. V.; Yanez, C. O.; Hernandez, F. E.; Przhonska, O. V. *J. Mater. Chem.* **2009**, *19*, 7498–7502.
(22) An, Z. S.; Odom, S. A.; Kelley, R. F.; Huang, C.; Zhang, X.; Barlow, S.; Padilha, L. A.; Fu, J.; Webster, S.; Hagan, D. J.; Van Stryland, E. W.; Wasielewski, S. M. R.; Marder, S. R. *J. Phys. Chem. A* **2009**, *113*, 5585–5593.
(23) Akoudad, S.; Roncali, J. *Synth. Met.* **1999**, *101*, 149.
(24) Mee, S. P. H.; Lee, V.; Baldwin, J. E. *Angew. Chem., Int. Ed. Engl.* **2004**, *43*, 1132–1136.
(25) Espinet, P.; Echavarren, A. M. *Angew. Chem., Int. Ed. Engl.* **2004**, *43*, 4704–4734.
(26) Stille, J. K. *Angew. Chem., Int. Ed. Engl.* **1986**, *25*, 508–524.
(27) Admassie, S.; Inganas, O.; Mammo, W.; Perzon, E.; Andersson, M. R. *Synth. Met.* **2006**, *156*, 614–623.
(28) Steckler, T. T.; Abboud, K. A.; Craps, M.; Rinzler, A. G.; Reynolds, J. R. *Chem. Commun.* **2007**, 4904–4906.
(29) Jenekhe, S. A.; Lu, L. D.; Alam, M. M. *Macromolecules* **2001**, *34*, 7315–7324.
(30) Gong, Y.; Guo, X.; Wang, S.; Su, H.; Xia, A.; He, Q.; Bai, F. *J. Phys. Chem. A* **2007**, *111*, 5806–5812.
(31) Beaujuge, P. M.; Amb, C. M.; Reynolds, J. R. *Acc. Chem. Res.* **2010**, *43*, 1396–1407.
(32) Beaujuge, P. M.; Ellinger, S.; Reynolds, P. D. J. R. *Adv. Mater.* **2008**, *20*, 2772–2776.
(33) Pritchett, T. M.; Sun, W. F.; Zhang, B. G.; Ferry, M. J.; Li, Y. J.; Haley, J. E.; Mackie, D. M.; Shensky, W.; Mott, A. G. *Opt. Lett.* **2010**, *35*, 1305–1307.
(34) Lim, J. H.; Przhonska, O. V.; Khodja, S.; Yang, S.; Ross, T. S.; Hagan, D. J.; Van Stryland, E. W.; Bondar, M. V.; Slominsky, Y. L. *Chem. Phys.* **1999**, *245*, 79–97.
(35) Siebrand, W. *J. Chem. Phys.* **1966**, *44*, 4055–4057.
(36) Siebrand, W. *J. Chem. Phys.* **1967**, *46*, 440–447.
(37) Wang, J.-L.; Xiao, Q.; Pei, J. *Org. Lett.* **2010**, *12*, 4164–4167.
(38) Lopez Arbeloa, I.; Rohatgi-Mukherjee, K. K. *Chem. Phys. Lett.* **1986**, *129*, 607–614.
(39) Lebedev, A. Y.; Filatov, M. A.; Cheprakov, A. V.; Vinogradov, S. A. *J. Phys. Chem. A* **2008**, *112*, 7723–7733.
(40) Sheik-Bahae, M.; Said, A. A.; Stryland, E. W. V. *Opt. Lett.* **1989**, *14*, 955–957.
(41) Sheik-Bahae, M.; Said, A. A.; Wei, T.-H.; Hagan, D. R.; Stryland, E. W. V. *IEEE J. Quantum Electron.* **1990**, *26*, 760–769.
(42) Xu, C.; Webb, W. W. *J. Opt. Soc. Am. B: Opt. Phys.* **1996**, *13*, 481–491.
(43) Pawlicki, M.; Collins, H. A.; Denning, R. G.; Anderson, H. L. *Angew. Chem., Int. Ed.* **2009**, *48*, 3244–3266.
(44) Albota, M.; Beljonne, D.; Brédas, J.-L.; Ehrlich, J. E.; Fu, J.-Y.; Heikal, A. A.; Hess, S. E.; Kogej, T.; Levin, M. D.; Marder, S. R.; McCord-Maughon, D.; Perry, J. W.; Röckel, H.; Rumi, M.; Subramaniam, G.; Webb, W. W.; Wu, X.-L.; Xu, C. *Science* **1998**, *281*, 1653–1656.
(45) Cronstrand, P.; Luo, Y.; Agren, H. *Chem. Phys. Lett.* **2002**, *352*, 262–269.
(46) Monson, P. R.; McClain, W. M. *J. Chem. Phys.* **1970**, *53*, 29–37.
(47) Birge, R. R.; Bennett, J. A.; Pierce, B. M.; Thomas, T. M. *J. Am. Chem. Soc.* **1978**, *100*, 1533–1539.
(48) Fu, J.; Padilha, L. A.; Hagan, D. J.; Van Stryland, E. W.; Przhonska, O. V.; Bondar, M. V.; Slominsky, Y. L.; Kachkovski, A. D. *J. Opt. Soc. Am. B: Opt. Phys.* **2007**, *24*, 56–66.
(49) Rumi, M.; Ehrlich, J. E.; Heikal, A. A.; Perry, J. W.; Barlow, S.; Hu, Z. Y.; McCord-Maughon, D.; Parker, T. C.; Rockel, H.; Thayumanavan, S.; Marder, S. R.; Beljonne, D.; Bredas, J. L. *J. Am. Chem. Soc.* **2000**, *122*, 9500–9510.
(50) Webster, S.; Fu, J.; Padilha, L. A.; Przhonska, O. V.; Hagan, D. J.; Van Stryland, E. W.; Bondar, M. V.; Slominsky, Y. L.; Kachkovski, A. D. *Chem. Phys.* **2008**, *348*, 143–151.
(51) Webster, S.; Padilha, L. A.; Hu, H.; Przhonska, O. V.; Hagan, D. J.; Stryland, E. W. V.; Bondar, M. V.; Davydenko, I. G.; Slominsky, Y. L.; Kachkovski, A. D. *J. Lumin.* **2008**, *128*, 1927–1936.
(52) Thompson, B. C.; Kim, Y. G.; McCarley, T. D.; Reynolds, J. R. *J. Am. Chem. Soc.* **2006**, *128*, 12714–12725.
(53) Van Mullekom, H. A. M.; Vekemans, J. A. J. M.; Meijer, E. W. *Chem.—Eur. J.* **1998**, *7*, 1235–1242.
(54) DuBois, C. J.; Abboud, K. A.; Reynolds, J. R. *J. Phys. Chem. B* **2004**, *108*, 8550–8557.
(55) Bredas, J. L.; Silbey, R.; Boudreaux, D. S.; Chance, R. R. *J. Am. Chem. Soc.* **1983**, *105*, 6555–6559.
(56) Ozen, A. S.; Atilgan, C.; Sonmez, G. *J. Phys. Chem. C* **2007**, *111*, 16362–16371.
(57) Wu, C. C.; Sturm, J. C.; Register, R. A.; Tian, J.; Dana, E. P.; Thompson, M. E. *IEEE Trans. Electron Devices* **1997**, *44*, 1269–1281.
(58) Cleave, V.; Yahioglu, G.; Le Barny, P.; Hwang, D. H.; Holmes, A. B.; Friend, R. H.; Tessler, N. *Adv. Mater.* **2001**, *13*, 44–47.
(59) The views and conclusions contained in this document are those of the authors and should not be interpreted as representing the official policies, either expressed or implied, of the Defense Advanced Research Projects Agency; the U.S. Army Aviation and Missile Research, Development, and Engineering Center; or the U.S. Government.